Radiology

CT-based Radiogenomic Analysis of Clinical Stage I Lung Adenocarcinoma with Histopathologic Features and Oncologic Outcomes

Rocio Perez-Johnston, MD • Jose A. Araujo-Filho, MD, PhD • James G. Connolly, MD • Raul Caso, MD • Karissa Whiting, MS • Kay See Tan, PhD • Jian Zhou, MD • Peter Gibbs, PhD • Natasha Rekhtman, MD, PhD • Michelle S. Ginsberg, MD • David R. Jones, MD

From the Department of Radiology (R.P., J.A.A., P.G., M.S.G.), Druckenmiller Center for Lung Cancer Research (R.P., K.S.T., N.R., M.S.G., D.R.J.), Thoracic Surgery Service (J.G.C., R.C., J.Z., D.R.J.), Biostatistics Service, Department of Epidemiology and Biostatistics (K.W., K.S.T.), and Department of Pathology (N.R.), Memorial Sloan Kettering Cancer Center, 1275 York Ave, Box 7, New York, NY 10065. Received June 23, 2021; revision requested August 9; revision received November 10; accepted December 9. **Address correspondence to** D.R.J. (e-mail: *jonesd2@mskcc.org*).

Memorial Sloan Kettering Cancer Center supported by the National Cancer Institute (P30 CA008748). J.G.C. supported by the National Cancer Institute (T32CA009501). D.R.J. supported by the National Cancer Institute (R01CA217169, R01CA240472), Hamilton Family Foundation, and Al-Asmakh Charity Foundation.

Conflicts of interest are listed at the end of this article.

See also the editorial by Nishino in this issue.

Radiology 2022; 303:664–672 • https://doi.org/10.1148/radiol.211582 • **Content code:** CH

Background: A preoperative predictive model is needed that can be used to identify patients with lung adenocarcinoma (LUAD) who have a higher risk of recurrence or metastasis.

Purpose: To investigate associations between CT-based radiomic consensus clustering of stage I LUAD and clinical-pathologic features, genomic data, and patient outcomes.

Materials and Methods: Patients who underwent complete surgical resection for LUAD from April 2014 to December 2017 with preoperative CT and next-generation sequencing data were retrospectively identified. Comprehensive radiomic analysis was performed on preoperative CT images; tumors were classified as solid, ground glass, or mixed. Patients were clustered into groups based on their radiomics features using consensus clustering, and clusters were compared with tumor genomic alterations, histopathologic features, and recurrence-specific survival (Kruskal-Wallis test for continuous data, χ^2 or Fisher exact test for categorical data, and log-rank test for recurrence-specific survival). Cluster analysis was performed on the entire cohort and on the solid, ground-glass, and mixed lesion subgroups.

Results: In total, 219 patients were included in the study (median age, 68 years; interquartile range, 63–74 years; 150 [68%] women). Four radiomic clusters were identified. Cluster 1 was associated with lepidic, acinar, and papillary subtypes (76 of 90 [84%]); clusters 2 (13 of 50 [26%]) and 4 (13 of 45 [29%]) were associated with solid and micropapillary subtypes ($P < .001$). The *EGFR* alterations were highest in cluster 1 (38 of 90 [42%], $P = .004$). Clusters 2, 3, and 4 were associated with lymphovascular invasion (19 of 50 [38%], 14 of 34 [41%], and 28 of 45 [62%], respectively; $P < .001$) and tumor spread through air spaces (32 of 50 [64%], 21 of 34 [62%], and 31 of 45 [69%], respectively; $P < .001$). *STK11* alterations (14 of 45 [31%]; $P = .006$), phosphoinositide 3-kinase pathway alterations (22 of 45 [49%], $P < .001$), and risk of recurrence (log-rank $P < .001$) were highest in cluster 4.

Conclusion: CT-based radiomic consensus clustering enabled identification of associations between radiomic features and clinical-pathologic and genomic features and outcomes in patients with clinical stage I lung adenocarcinoma.

Online supplemental material is available for this article.

Lung cancer is the leading cause of cancer-related death, with non–small cell lung cancer (NSCLC) accounting for 85% of cases of lung cancer, and adenocarcinoma representing the predominant histologic subtype (1). A hallmark of lung adenocarcinoma (LUAD) is its heterogeneity of histologic subtypes and tumor genomic profiles. This heterogeneity results in variable prognostic challenges, patient outcomes, and responses to antineoplastic therapy. Heretofore, the single most important prognostic factor for LUAD has been tumor-node-metastasis classification (2). However, there are limitations to stratifying patients according to this metric alone. Patients with the same pathologic stage may have differences in recurrence and survival after resection of NSCLC, especially with the use of targeted therapy and immunotherapy in the neoadjuvant and adjuvant settings (3,4). Therefore, there is a need for a preoperative predictive model that can enable better identification of patients with higher risk for recurrent or metastatic disease based on known clinical-pathologic and genomic features (3,5–9).

Helical CT imaging has become a mainstay for lung cancer screening and treatment and monitoring of response to therapy (10). Unlike fluorodeoxyglucose PET, CT does not allow assessment of the relative metabolism of the thoracic lesion; however, it does provide an effective means of preoperatively and noninvasively assessing tumor radiomic features. Radiomics comprises automated or semiautomated high-throughput extraction of large

Abbreviations

IQR = interquartile range, LUAD = lung adenocarcinoma, LVI = lymphovascular invasion, NGS = next-generation sequencing, NSCLC = non–small cell lung cancer, PI3K = phosphoinositide 3-kinase, RSS = recurrence-specific survival, STAS = spread though air spaces

Summary

CT-based radiomic features were significantly associated with prognostic histopathologic features, specific genomic alterations, and recurrence-specific survival in patients with clinical stage I lung adenocarcinoma.

Key Results

- This retrospective analysis of 219 patients with completely resected clinical stage I lung adenocarcinoma evaluated four clusters of CT-based radiomics features.
- Histologic subtypes were associated with clusters: cluster 1 was associated with lepidic, acinar, and papillary subtypes (84%), whereas clusters 2 (26%) and 4 (29%) were associated with solid and micropapillary subtypes ($P = .001$); in addition, the frequency of the poor prognosis histologic factor lymphovascular invasion was highest in cluster 4 (62%, $P < .001$), and the frequency of spread though air spaces was higher in clusters 2 (64%), 3 (62%), and 4 (69%) than in cluster 1 (30%) ($P < .001$).
- Genomic alterations varied by cluster: A higher frequency of *EGFR* alterations was noted in cluster 1 (42%, $P = .004$), whereas *STK11* alterations (31%, $P = .006$), phosphoinositide 3-kinase pathway alterations (49%, $P < .001$), and risk of recurrence (log-rank $P < .001$; 2-year residual sum of squares probability cluster 4, 74% [95% CI: 61, 88]) were highest in cluster 4.

amounts of quantifiable information from radiologic imaging, which, when combined with genomic data, can identify tumor-inherited phenotypes for potential prognostication of disease and prediction of response to therapy (11–13). The utility of radiomics for the discrimination of benign and malignant thoracic nodules, as well as for classification of LUAD histologic subtypes, has been established (14,15).

With the increasingly widespread use of next-generation sequencing (NGS) in the treatment of NSCLC, we believe that radiomic and genomic data can be leveraged to more effectively predict lung cancer outcomes. However, there is a paucity of studies investigating the feasibility of radiogenomics for the preoperative stratification of patients with LUAD. To bridge this knowledge gap, we investigated the associations among consensus clusters obtained from radiomic analysis of segmented LUAD lesions to determine the associations between clinicopathologic and genomic data and patient outcomes.

Materials and Methods

Study Sample

After we obtained institutional review board approval and in compliance with the Health Insurance Portability and Accountability Act of 1996, we retrospectively identified all consecutive patients who underwent complete surgical resection for LUAD from April 2014 to December 2017 and had NGS performed on the tumor (16). Clinical-pathologic data recorded included smoking history, clinical stage, tumor recurrence, lymphovascular invasion (LVI), spread through air spaces (STAS), and nodal status. Recurrences were distinguished from metachronous tumors using the Martini and Melamed criteria, with confirmation from pathologic and genomic relatedness, when available (17). LUAD histologic subtypes were classified using the eighth edition of the American Joint Committee on Cancer Staging Manual (18) and the International Association for the Study of Lung Cancer classification system (1). Our inclusion criteria included patients with clinical stage I LUAD who underwent complete surgical resection (R0) and had preoperative CT and NGS data. Exclusion criteria included adjuvant induction therapy, incomplete resection (R1 or R2 resections), CT scans without thin sections, and parenchymal findings adjacent to the tumor that precluded segmentation, such as lung collapse. In total, 219 patients with completely resected clinical stage I LUAD met the inclusion criteria. The study design and results reporting were performed in accordance with the Strengthening the Reporting of Observational Studies in Epidemiology reporting guidelines (19).

Clinical Outcome

The primary end point was recurrence-specific survival (RSS), which was defined as the time from surgery to recurrence in the lung or spread to other organs and was otherwise censored at the time of death or last follow-up. Follow-up ranged from 0.29 to 4.44 years. RSS probabilities were calculated 1 and 2 years after surgery.

Tumor Genomic Analysis

Broad-based NGS was performed and analyzed, as previously described (6,16). Tumor mutational burden was defined as the fraction of nonsynonymous single-nucleotide or insertion or deletion mutations divided by the length of the coding region (in megabases) sequenced by each panel (0.98, 1.06, and 1.22 Mb in the 341-, 410-, and 468-gene panels, respectively). The fraction of genome altered was defined as the fraction of $\log_2$ copy number variation (gain or loss) greater than 0.2 divided by the size of the genome, of which the copy number was profiled.

Genes altered in 15% or more of the data set (*EGFR*, *KRAS*, *TP53*, *RBM10*, and *STK11*) and gene mutations with targetable therapies in LUAD (*BRAF*, *ALK*, and *ROS1*) were examined. The 10 canonical oncogenic signaling pathways were investigated, as previously described (6,20). In total, 121 genes were identified at the intersection of the a priori pathway templates (21) and the NGS panel (16). Analysis of specific somatic alterations was performed using OncoKB *(https://www.oncokb.org/)* to remove variants of unknown importance and to identify activating oncogenes or inactivating tumor-suppressor genes (22).

CT Image Acquisition

All patients underwent multisection CT performed as part of standard clinical care for suspicion or staging of pulmonary malignancy. Most CT studies ($n = 157$ [72%]) were performed at our institution (Lightspeed VCT, Discovery CT 750HD; GE Healthcare); the remaining studies ($n = 62$ [28%]) were performed at outside institutions (GE, Siemens, Philips) and were submitted and uploaded to our picture archiving and communication system. In total, 112 (51%) studies were contrast enhanced, and dose-length product ranged from 171 to 587 mGy · cm. Section thickness varied from 0.6 to 2 mm. Axial series were deidentified and up-

loaded to ITK-SNAP, version 3.8.0-beta *(http://www.itksnap.org)* for segmentation analysis.

Nodule Segmentation and Radiomic Features

The target lesions were identified and classified independently by a thoracic radiologist (R.P. or J.A.A., each with 3 years of experience) in accordance with the classification protocol proposed by Suzuki et al (23). The radiologists were blinded to all clinical and outcome information. Tumors were manually segmented after consensus was reached between the thoracic radiologist (J.A.A.) and the oncologic surgeons (R.C., J.Z. [in training]) and in consensus with a senior thoracic radiologist (M.S.G., 25 years of experience), who adjudicated any disagreements among the initial readers. Tumor regions of interest were defined using open-source software (ITK-SNAP; *http://www.itksnap.org/pmwiki/pmwiki.php*), using the lung window setting across all two-dimensional sections in the axial view, including bronchi, blood vessels, and vacuoles within the nodules and excluding normal lung tissue, chest wall, and mediastinal structures. When nodules were near the mediastinum or chest wall, the option to vary the window and level setting was selected to properly annotate nodule borders.

Quantitative Texture Analysis and Consensus Clustering

A total of 102 quantitative features were extracted using Computational Environment for Radiological Research (24), which has recently been shown to conform with the image biomarker standardization initiative (25). Consensus clustering was used to construct a radiomic signature that separated tumors by their similarities and differences in texture features (P.G.). We next grouped tumors based on region of interest definitions into the following categories: *(a)* solid (more than 90% of the lesion is solid), *(b)* ground glass (less than 10% of the lesion is solid), and *(c)* mixed lesion (10%–90% of the lesion is solid).

Consensus clustering (R software, version 1.56.0, ConsensusClusterPlus package; R Foundation for Statistical Computing)—a data-driven method to determine the number and membership of possible clusters in a data set—was used to cluster patients based on the radiomics features of their lesions (K.W., K.S.T.). This method is a data-driven approach to identify an appropriate number of clusters *(k)* in the data, a value that is otherwise often chosen arbitrarily in unsupervised clustering analyses. By assessing cluster agreement across multiple iterations of a clustering algorithm on multiple subsamples of the data, an optimal *k* value that corresponds to well-separated and stable clusters is selected. To implement the method, for a given set of possible values of *k* (we tested values between 1 and 6), we iteratively subsampled 80% of the data set, hierarchically clustered each subsample, and then assessed the relative frequency that each patient was clustered with each other patient for each value of *k*, resulting in a consensus matrix. For each *k* value, we could then compute the change in area under the cumulative distribution function curve of the consensus matrix distribution, which showed how well separated the clusters were. We chose an optimal *k* value that corresponded to a sharp decrease in this change in area under the receiver operating characteristic curve, which indicated further gains in separability were negligible after that *k* value. We used a hierarchical clustering algorithm within the ConsensusClusterPlus framework in this study, but any clustering algorithm can be used. Cluster analysis was performed in the entire cohort (n = 219), as well as in the solid (n = 107), ground-glass (n = 54), and mixed (n = 58) subgroups.

Statistical Analyses

Statistical analyses were performed to determine whether resulting cluster membership was associated with clinical features, CT findings (including lesion centrality, focality, and percentage composition of the lesion components), pathologic features (histologic subtype, LVI, and STAS), and tumor genomic features (K.W., K.S.T.). A *k* value of 4 was chosen to split the data based on the relative change in the area under the

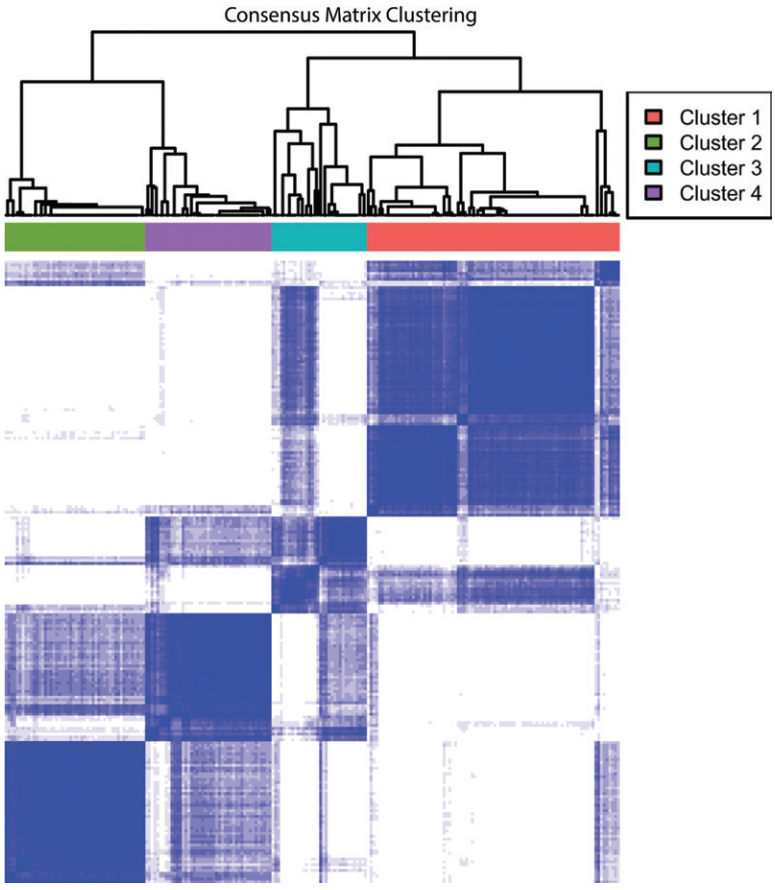

Figure 1: Conditional density function demonstrating consensus clustering of radiomic features at a *k* value of 4. For a set of possible *k* values of 1–6, we iteratively subsampled 80% of the data set, hierarchically clustered each subsample, and then assessed the relative frequency that each patient was clustered with each other patient for each *k* value, resulting in a consensus matrix. For each *k* value, we then computed the change in area under the cumulative distribution function curve of the consensus matrix distribution, which showed how well separated the clusters were. We chose an optimal *k* value that corresponded to a sharp decrease in this change in area under the receiver operating characteristic curve, which indicated that further gains in separability were negligible after that *k* value.

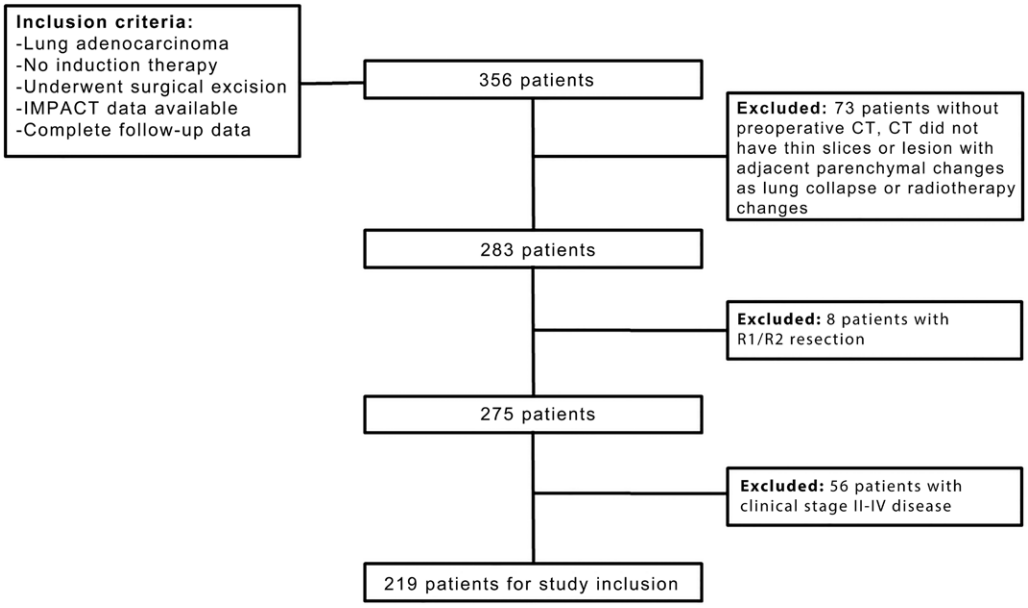

Figure 2: Consort diagram. IMPACT = Integrated Mutation Profiling of Actionable Cancer Targets.

conditional density function curve (Fig 1). Clinical characteristics of the final clusters were compared using the Fisher exact test or the χ^2 test for categorical data and the Kruskal-Wallis test for continuous data. RSS was defined as the time from surgery to first recurrence and was otherwise censored at the time of last follow-up or death for patients without a recurrence. RSS was analyzed using Kaplan-Meier curves, and differences in RSS between groups were assessed using log-rank tests. RSS estimates at 2 years after surgery are provided along with 95% CIs. The median and range of follow-up was calculated among patients still alive at the end of the study. Statistical analyses were repeated within the individual subgroups of solid lesions, ground-glass lesions, and mixed lesions. R software, version 3.6.1 (R Foundation for Statistical Computing), was used for all analyses. All hypothesis tests were two sided, and $P < .05$ indicated a significant difference.

Results

Patient and Tumor Characteristics

Of 356 patients identified with LUAD, 219 met the inclusion criteria (137 were excluded) (Fig 2). Median age was 68 years (interquartile range [IQR], 63–74 years), and 150 patients (68%) were women and 69 (32%) were men. Most patients were current (n = 22 [10%]) or former (n = 151 [69%]) smokers. All patients had an R0 resection; the most frequent procedure was lobectomy (n = 104 [47%]), followed by wedge resection (n = 89 [41%]), segmentectomy (n = 24 [11%]), and pneumonectomy (n = 2 [1%]). Most lesions on CT images were solid (n = 107 [49%]), followed by mixed (n = 58 [26%]) and ground glass (n = 54 [25%]). Twenty-five (11%) patients had node-positive disease and 194 (89%) had node-negative disease (Table 1). Among patients with recorded presence of STAS (n = 149), STAS was present in 111 (74%) samples, whereas among pa-

Table 1: Patient and CT Characteristics

Characteristic	Finding (n = 219)
Median age at surgery (y)*	68 (63–74)
Sex	
Female	150 (68)
Male	69 (32)
Smoking history	
Current	22 (10)
Former	151 (69)
Never	46 (21)
Median CT size (cm)*	1.8 (1.3–2.73)
CT location	
Right upper lobe	63 (29)
Right middle lobe	15 (7)
Right lower lobe	52 (24)
Left upper lobe	49 (22)
Left lower lobe	39 (18)
Multiple	1 (0)
CT texture classification	
Solid	107 (49)
Ground glass	54 (25)
Mixed	58 (26)
Clinical stage	
IA1	22 (10)
IA2	119 (54)
IA3	62 (28)
IB	16 (7)
Pathologic nodal status	
Positive	25 (11)
Negative	194 (89)

Note.—Unless otherwise indicated, data are numbers of patients and data in parentheses are percentages.
* Data in parentheses are the interquartile range.

tients with recorded presence of LVI (n = 215), LVI was present in only 73 (34%) samples (Table 2).

The median tumor mutational burden was 4.9 (IQR, 2.1–8.8), and the median fraction of genome altered was 3 (IQR, 0–9). The most frequently altered genes were *KRAS* (n = 92 [42%]), *TP53* (n = 72 [33%]), *EGFR* (n = 66 [30%]), and *STK11* (n = 33 [15%]). The most frequently altered oncogenic pathways were receptor tyrosine kinase-Ras (n = 188 [86%]), p53 (n = 84 [38%]), and phosphoinositide 3-kinase (PI3K) (n = 51 [23%]).

Table 2: Tumor Histologic and Pathologic Characteristics

Characteristic	No. of Findings
Predominant subtype (n = 219)	
AIS	3 (1)
MIA	2 (1)
Lepidic	39 (18)
Acinar or papillary	123 (56)
Micropapillary or solid	34 (16)
Mixed	15 (7)
Other	3 (1)
STAS (n = 149)	
Present	111 (74)
Not present	38 (26)
LVI (n = 215)	
Present	73 (34)
Not present	142 (66)

Note.—Data in parentheses are percentages. AIS = adenocarcinoma in situ, LVI = lymphovascular invasion, MIA = microinvasive adenocarcinoma, STAS = spread though air spaces.

Clinical Outcome

Median follow-up for all patients was 2.19 years (range, 0.29–4.44 years); 29 recurrences and 20 deaths were recorded (six deaths with no prior recurrence). Solid lesions were associated with worse RSS (2-year RSS, 82%; 95% CI: 74, 90), compared with ground-glass (2-year RSS, 98%; 95% CI: 94, 100; log-rank $P < .001$) and mixed (2-year RSS, 95%; 95% CI: 89, 100) lesions. In addition, lesions with LVI (2-year RSS = 75%; 95% CI: 65, 86), lesions without LVI (2-year RSS = 97%; 95% CI: 93, 100; log-rank $P < .001$), lesions with STAS (2-year RSS = 89%; 95% CI: 83, 96), lesions without STAS (2-year RSS, 97%; 95% CI: 93, 100; log-rank $P = .047$), and lesions with nodal involvement (N+: 2-year RSS = 49%; 95% CI: 33, 75; N0: 2-year RSS = 94%; 95% CI: 91, 98; log-rank $P < .001$) were associated with worse RSS (Fig E1 [online]).

For cluster analysis in the solid subgroup (n = 107), median follow-up was 2.25 years (range, 0.29–4.44 years); 24 recurrences and 17 deaths were recorded in this subgroup. Median follow-up was 2.11 years (range, 0.51–4.34 years) for the ground-glass subgroup (n = 54) and 2.18 years (range, 0.58–4.24 years) for the mixed subgroup (n = 58).

Consensus Clustering Associations

For all patients, consensus clustering based on all computed textural features showed a sharp decrease in the relative change in area under the conditional density function curve at a k value of 4. Demographic, morphologic, and histologic data grouped into clusters are summarized in Table 3. Cluster 1 had a higher frequency of lepidic, acinar, and papillary subtypes (76 of 90 [84%]) compared with clusters 2 and 4, which had a higher frequency of solid and micropapillary subtypes (cluster 2, 13 of 50 [26%]; cluster 4, 13 of 45 [29%]; $P < .001$) (Fig 3). Similarly,

Table 3: Demographic, Morphologic, and Histologic Characteristics by Cluster

Characteristic	All (n = 219)	Cluster 1 (n = 90)	Cluster 2 (n = 50)	Cluster 3 (n = 34)	Cluster 4 (n = 45)	P Value*
Median age (y)†	68 (63–74)	69 (65–74)	70 (62–74)	66 (60–74)	66 (61–72)	.3
Sex						.3
Female	150 (68)	65 (72)	29 (58)	25 (74)	31 (69)	…
Male	69 (32)	25 (28)	21 (42)	9 (26)	14 (31)	…
Location						.3
Central	12 (5)	3 (3)	2 (4)	4 (12)	3 (7)	…
Peripheral	207 (94)	87 (97)	48 (96)	30 (88)	42 (93)	…
Tumor type						<.001
Solid	107 (49)	5 (6)	50 (100)	13 (38)	39 (87)	...
Pure ground-glass opacity	54 (25)	47 (52)	0	7 (21)	0	…
Mixed	58 (26)	38 (42)	0	14 (41)	6 (13)	…
Median CT size (cm)†	1.8 (1.3–2.3)	1.7 (1.3–2.18)	1.4 (1.2–2.18)	1.8 (1.33–2.5)	2.1 (1.5–2.7)	.010
Histologic subtype						<.001
Lepidic, acinar, or papillary	162 (74)	76 (84)	33 (66)	25 (74)	28 (62)	…
Micropapillary or solid	34 (16)	4 (4)	13 (26)	4 (12)	13 (29)	…
Unknown	23 (10)	10 (11)	4 (8)	5 (15)	4 (9)	…

Note.—Unless otherwise indicated, data in parentheses are percentages.

* Fisher exact test or Pearson χ^2 test were used for categorical variables (sex, location, characteristic, histologic type); Kruskal-Wallis test was used for continuous variables (CT size, age).

† Data in parentheses are the interquartile range.

Figure 3: OncoPrint of clinical-pathologic and genomic variables for all patients with clinical stage I lung adenocarcinoma broken down by radiomic consensus clustering. Columns represent patients within each cluster of radiomics features, and rows represent the frequencies of alterations of all individually analyzed oncogenic genes and 10 canonical oncogenic pathways. Cluster characteristics were compared using Fisher or χ^2 exact test for categorical data and Kruskal-Wallis test for continuous data. * Associations between radiomic clusters and clinicopathologic or genomic variables are significant ($P < .05$). FGA = fraction of genome altered, LVI = lymphovascular invasion, NA = not applicable, MIP = micropapillary, SOL = solid, STAS = spread through air spaces, TMB = tumor mutational burden.

the frequency of LVI was highest in cluster 4 (28 of 45 [62%]) ($P < .001$), and the frequency of STAS was higher in clusters 2 (32 of 50 [64%]), 3 (21 of 34 [62%]), and 4 (31 of 45 [69%]) than in cluster 1 (27 of 90 [30%], $P < .001$) (Fig 3). Cluster 4 had the highest median fraction of genome altered (7 [IQR = 1–14], $P = .020$) and the highest frequency of PI3K pathway alterations (22 of 45 [49%], $P < .001$) and *STK11* alterations (14 of 45 [31%], $P = .006$). Cluster 1 had the highest frequency of *EGFR* alterations (38 of 90 [42%], $P = .004$) (Fig 3). Examples of cases per cluster are shown in Figure 4. Clusters 3 and 4 had worse RSS than did clusters 1 and 2 (2-year RSS probability: cluster 1, 98% [95% CI: 95, 100]; cluster 2, 91% [95% CI: 83, 100]; cluster 3, 83% [95% CI: 69, 100]; cluster 4, 74% [95% CI: 61, 88]; log-rank $P < .001$) (Fig 5).

At cluster analysis in the solid subgroup ($n = 107$), we found no evidence of a difference in histologic subtype ($P = .7$) or STAS ($P = .2$) among clusters. The frequency of LVI was highest in cluster 4 (33 of 47 [70%], $P < .001$) (Fig E2 [online]). Cluster 4 had the highest median fraction of genome altered (7 [IQR = 2–15], $P = .014$). Cluster 3 had a higher frequency of PI3K pathway alterations (seven of 11 [64%], $P = .005$) and *STK11* alterations (seven of 11 [64%], $P = .002$) compared with the other clusters (Fig E2 [online]). In addition, clusters 2 (36 of 39 [92%]), 3 (10 of 11 [91%]), and 4 (45 of 47 [96%]) had a higher frequency of receptor tyrosine kinase-Ras alteration than did cluster 1 (eight of 10 [80%]) ($P = .03$). The 2-year RSS probability was 100% (95% CI: 100, 100) for cluster 1, 92% (95% CI: 84, 100) for cluster 2, 82% (95% CI: 62, 100) for cluster 3, and 68% (95% CI: 55, 84) for cluster 4, with the shortest RSS in cluster 4 ($P = .03$) (Fig E3 [online]).

In the ground-glass group ($n = 54$, conditional density function with $k = 4$), we found no evidence of a difference in histologic subtypes ($P = .5$); lepidic, acinar, or papillary subtypes were present in 17 of 19 patients (89%) in cluster 1, six of 10 patients (60%) in cluster 2, 13 of 16 patients (81%) in cluster 3, and eight of nine patients (89%) in cluster 4; micropapillary and solid subtypes were seen in only one patient in clusters 1 and 2. Similarly, STAS ($P = .3$), LVI ($P = .2$), genomic alterations ($P > .05$), and RSS ($P \geq .9$) were not significantly different between clusters.

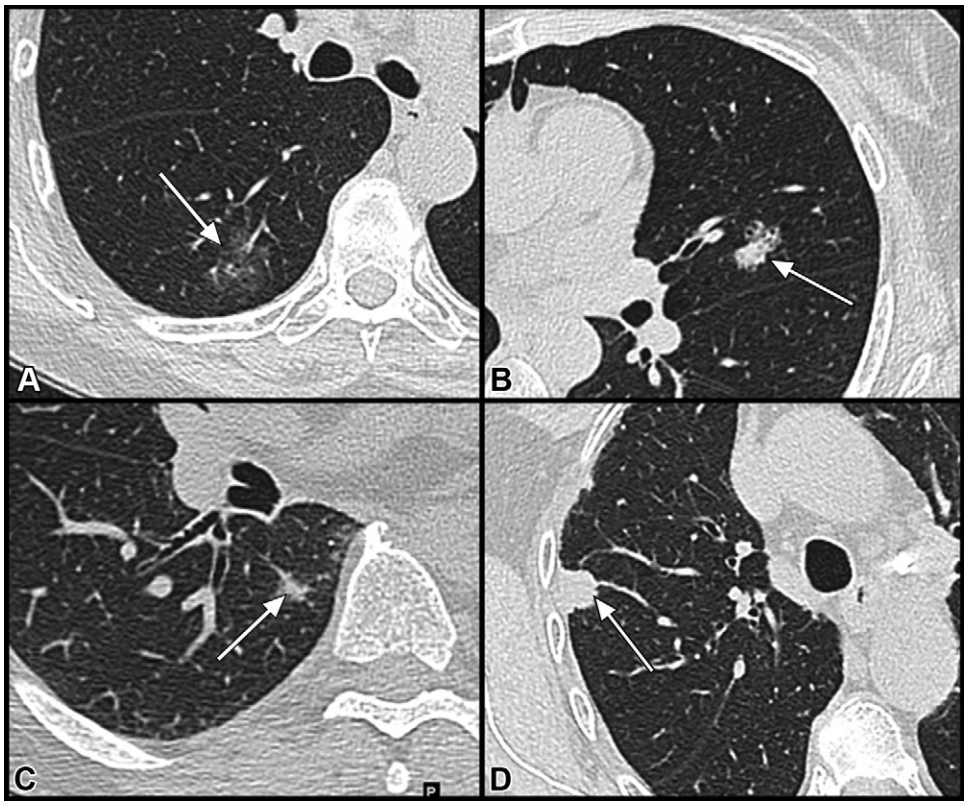

Figure 4: Thin-section CT images of lesions used for radiomic cluster analysis. **(A)** Cluster 1. Ground-glass nodule in the right lower lobe (arrow) measuring 2.2 cm, predominantly lepidic histologic subtype, *EGFR*, and phosphoinositide 3-kinase (pPI3K) positive. Follow-up was 35 months without evidence of recurrence. **(B)** Cluster 2. Part-solid nodule in the left upper lobe (arrow) measuring 2.1 cm, solid and micropapillary histologic subtype, spread through air spaces (STAS) positive, *STK11* and *KRAS* positive. Follow-up was 40 months without evidence of recurrence. **(C)** Cluster 3. Solid nodule (arrow) with thin ground-glass halo in the right lower lobe measuring 1.0 cm; solid and micropapillary histologic subtype; STAS positive; TP53, pPI3K, and receptor tyrosine kinase-Ras positive. The patient underwent right lower lobe wedge resection and was diagnosed with recurrence 9 months after resection. **(D)** Cluster 4. Solid nodule (arrow) in the right upper lobe measuring 1.4 cm; solid and micropapillary histologic subtype; STAS and lymphovascular invasion positive; *STK11*, *KRAS*, and pPI3K positive. The patient underwent right upper lobectomy and was diagnosed with recurrence 15 months after resection.

In the mixed group (n = 58, conditional density function with k = 4), we found no evidence of a difference in histologic subtypes ($P > .9$); lepidic, acinar, or papillary subtypes were present in 12 of 15 patients (80%) in cluster 1, 14 of 16 patients (88%) in cluster 2, 18 of 22 patients (82%) in cluster 3, and five of five patients (100%) in cluster 4; micropapillary and solid subtypes were present in one case each in clusters 1, 2, and 3 and in zero cases in cluster 4. Similarly, no significant differences were found between clusters in terms of STAS (P = .2) or RSS (P = .49). A significant difference was observed for LVI: cluster 1 had the highest prevalence (seven of 15 [47%], P = .011), followed by clusters 2 (two of 16 [12%]), 3 (one of 22 [4%]), and 4 (zero of five [0%]). The only genomic alteration that was significantly different between clusters was *EGFR*, which was more prevalent in clusters 2 (11 of 16 [69%]) and 4 (three of five [60%]).

Discussion

The goal of this study was to determine, in patients with stage I lung cancer and next-generation sequencing (NGS), associations between clusters of CT-based radiomics features, histologic factors of poor prognosis, genomic alterations, and clinical outcomes (recurrence-specific survival [RSS]). When all patients were analyzed, cluster 1 was associated with less-aggressive histologic subtypes (lepidic, acinar, and papillary) and a higher frequency of *EGFR* alterations (42%, P = .004). Clusters 2 and 4 were associated with solid and micropapillary subtypes ($P < .001$); clusters 2, 3, and 4 were associated with lymphovascular invasion (LVI) (38%, 41%, and 62%, respectively; $P < .001$) and spread through air spaces (STAS) (64%, 62%, and 69%, respectively; $P < .001$). Cluster 4 had a higher frequency of *STK11* alterations (P = .006) and phosphoinositide 3-kinase (PI3K) pathway alterations ($P < .001$) and shorter RSS (log-rank $P < .001$). Within the solid subgroup, cluster 4 was associated with LVI ($P < .001$) and had the shortest RSS (log-rank P = .03); *STK11* alterations (P = .002) and PI3K pathway alterations (P = .005) were more frequent in cluster 3, and receptor tyrosine kinase-Ras alterations were more frequent in clusters 2, 3, and 4 (P = .03). Within the mixed subgroup, cluster 1 was associated with LVI (P = .011), and clusters 2 and 4 were associated with *EGFR* alteration

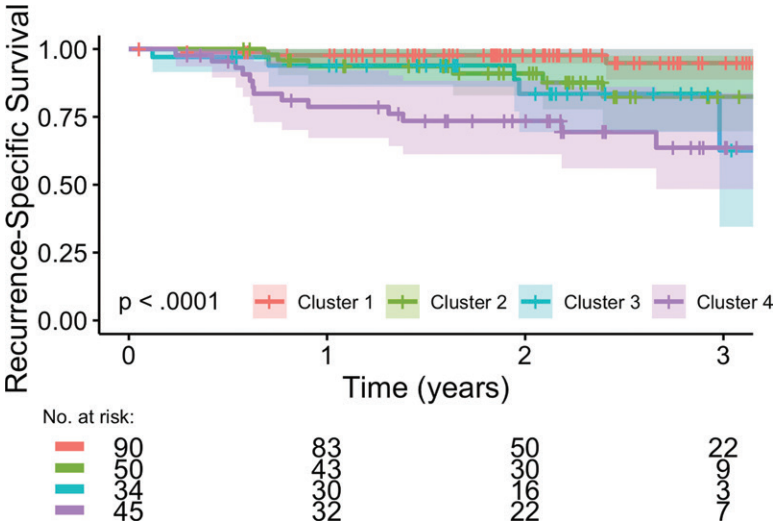

Figure 5: Two-year recurrence-specific survival for each of the four radiomic consensus clusters of the overall study cohort.

(P = .042); there was no evidence of an association with RSS, likely because of the few events within this subgroup. No significant results were found in the ground-glass subgroup.

Real-time applications of tumor NGS have been shown to be prognostic and predictive in patients with NSCLC (6–9). Our findings confirm that lepidic, acinar, and papillary histologic subtypes (more frequent in cluster 1) also had a higher frequency of *EGFR* alteration (P = .004), which was associated with longer RSS, compared with the other consensus clusters. Cluster 1 was represented by predominantly ground-glass and mixed lesions, whereas the remaining clusters were predominantly solid-type tumors. These findings agree with prior reports that indicate that ground-glass lesions may represent less-invasive disease and that *EGFR* alteration is associated with low-grade LUAD (26,27).

Radiomic features have been shown to have high sensitivity and moderate specificity to predict high-grade micropapillary and solid histologic subtype components (28). In our study, we confirmed that the more aggressive histologic subtypes (clusters 2 and 4) were associated with STAS ($P < .001$) and LVI ($P < .001$) and had a higher frequency of PI3K pathway alterations ($P < .001$) and *STK11* alterations (P = .006).

STK11 is a tumor-suppressor gene frequently mutated in NSCLC, and its mutation has been associated with local progression and metastatic dissemination (29). In our study, *STK11* alteration was associated with worse RSS in both the entire group (cluster 4, 74%; 95% CI: 61, 88) and the solid subgroup (cluster 3, 82%; 95% CI: 62, 100), similar to previous findings (30). Importantly, co-mutations of *KRAS/STK11* have recently been implicated to modulate resistance to immunotherapy in the setting of LUAD (31).

Alterations in the PI3K pathway were associated with solid tumors and shorter RSS. Deregulation of PI3K, which is an important signal transduction pathway involved in cell proliferation and differentiation, has been associated with aggressive and advanced-stage NSCLC (32). In addition, within the solid subgroup, the cluster with the worst prognosis, cluster 4, was associated with alterations in both the PI3K and the receptor tyrosine kinase-Ras pathway. Given the high rate of alteration of *KRAS* mutations in LUAD, recently developed KRASG12C inhibitors have shown promise in early clinical trials (33,34). Interestingly, resistance to these *KRAS* inhibitors has been suggested to be mediated through the PI3K pathway, which may blunt the therapeutic response and advance tumorigenesis (35,36).

Limitations of our study include the short median follow-up of 2 years. Additionally, as our institution benefits from specialty radiologic review of all clinical lung cancer cases, the reproducibility of our study and its clinical applications may be more challenging in a more diverse clinical setting. We also acknowledge that our sample size limited our ability to conduct a comprehensive analysis of the added value of the clusters. A natural extension of the reported results is to investigate the predictive value of the cluster membership. However, the necessary partition into training versus validation data sets was not possible given the limited sample size in this study. Additionally, multivariable modeling was not feasible in this setting because of the limited number of events (29 recurrences). Instead, we showed that patients can be grouped into meaningful risk profiles using these radiomics features alone, and these resulting groups correlate with clinical and genomic characteristics, which may provide insight into the prognostic interplay of clinical, pathologic, genomic, and imaging features. Future work is necessary to characterize and define the relationships between radiomics data and clinical factors, particularly tumor features, and baseline characteristics in a multivariable setting.

In conclusion, we have identified significant associations between CT-based radiomic features and known prognostic histologic factors, genomic drivers, and patient outcomes in a cohort of patients with operable clinical stage I lung adenocarcinoma. These associations were confirmed in the solid-type subgroup, in which additional associations with poor prognostic markers were also identified. Collectively, the mutual exclusivity from *EGFR* mutational status, the poor prognostic outcomes associated with alterations in *STK11* and the phosphoinositide 3-kinase pathway, and the known resistance to targeted therapies emphasize an unmet need for treatment and screening of solid-type clinical stage I disease. Early recognition of these features on CT images with radiomics has the potential to enable identification of patients with high risk, potentially tailoring surgical treatment and neoadjuvant targeted therapy and perhaps ultimately affecting the prognosis.

Acknowledgment: David B. Sewell, MA, MFA, of the Memorial Sloan Kettering Cancer Center Department of Surgery provided editorial assistance.

Author contributions: Guarantors of integrity of entire study, **R.P., J.A.A., R.C., K.W., J.Z., D.R.J.**; study concepts/study design or data acquisition or data analysis/interpretation, all authors; manuscript drafting or manuscript revision for important intellectual content, all authors; approval of final version of submitted

manuscript, all authors; agrees to ensure any questions related to the work are appropriately resolved, all authors; literature research, **R.P., J.A.A., R.C.**; clinical studies, **R.P., R.C., J.Z., D.R.J.**; statistical analysis, **K.W., K.S.T.**; and manuscript editing, **R.P., J.A.A., J.G.C., R.C., K.W., K.S.T., P.G., N.R., M.S.G., D.R.J.**

Disclosures of conflicts of interest: **R.P.** no relevant relationships. **J.A.A.** no relevant relationships. **J.G.C.** no relevant relationships. **R.C.** MedStar Georgetown University Hospital advisory board. **K.W.** no relevant relationships. **K.S.T.** no relevant relationships. **J.Z.** no relevant relationships. **P.G.** no relevant relationships. **N.R.** honoraria for serving on National Cancer Institute thoracic malignancies steering committee and as an associate editor for *Modern Pathology*. **M.S.G.** consulting fees from Ultimate Opinions in Medicine. **D.R.J.** consultant for AstraZeneca and on the Clinical Trial Steering Committee for Merck.

References

1. Travis WD, Brambilla E, Noguchi M, et al. International Association for the Study of Lung Cancer/American Thoracic Society/European Respiratory Society international multidisciplinary classification of lung adenocarcinoma. J Thorac Oncol 2011;6(2):244–285.
2. Chansky K, Sculier JP, Crowley JJ, et al. The International Association for the Study of Lung Cancer Staging Project: prognostic factors and pathologic TNM stage in surgically managed non–small cell lung cancer. J Thorac Oncol 2009;4(7):792–801.
3. Zhang J, Wu J, Tan Q, Zhu L, Gao W. Why do pathological stage IA lung adenocarcinomas vary from prognosis?: a clinicopathologic study of 176 patients with pathological stage IA lung adenocarcinoma based on the IASLC/ATS/ERS classification. J Thorac Oncol 2013;8(9):1196–1202.
4. Ost D, Goldberg J, Rolnitzky L, Rom WN. Survival after surgery in stage IA and IB non–small cell lung cancer. Am J Respir Crit Care Med 2008;177(5):516–523.
5. Dai C, Xie H, Su H, et al. Tumor Spread through Air Spaces Affects the Recurrence and Overall Survival in Patients with Lung Adenocarcinoma >2 to 3 cm. J Thorac Oncol 2017;12(7):1052–1060.
6. Zhou J, Sanchez-Vega F, Caso R, et al. Analysis of tumor genomic pathway alterations using broad-panel next-generation sequencing in surgically resected lung adenocarcinoma. Clin Cancer Res 2019;25(24):7475–7484.
7. Jones GD, Brandt WS, Shen R, et al. A genomic-pathologic annotated risk model to predict recurrence in early-stage lung adenocarcinoma. JAMA Surg 2021;156(2):e205601.
8. Jones GD, Caso R, Tan KS, et al. *KRAS* ^{G12C} Mutation Is Associated with Increased Risk of Recurrence in Surgically Resected Lung Adenocarcinoma. Clin Cancer Res 2021;27(9):2604–2612.
9. Caso R, Sanchez-Vega F, Tan KS, et al. The underlying tumor genomics of predominant histologic subtypes in lung adenocarcinoma. J Thorac Oncol 2020;15(12):1844–1856.
10. Eisenhauer EA, Therasse P, Bogaerts J, et al. New response evaluation criteria in solid tumours: revised RECIST guideline (version 1.1). Eur J Cancer 2009;45(2):228–247.
11. Chen B, Zhang R, Gan Y, Yang L, Li W. Development and clinical application of radiomics in lung cancer. Radiat Oncol 2017;12(1):154.
12. Dercle L, Fronheiser M, Lu L, et al. Identification of non–small cell lung cancer sensitive to systemic cancer therapies using radiomics. Clin Cancer Res 2020;26(9):2151–2162.
13. Lee G, Lee HY, Park H, et al. Radiomics and its emerging role in lung cancer research, imaging biomarkers and clinical management: State of the art. Eur J Radiol 2017;86:297–307.
14. She Y, Zhang L, Zhu H, et al. The predictive value of CT-based radiomics in differentiating indolent from invasive lung adenocarcinoma in patients with pulmonary nodules. Eur Radiol 2018;28(12):5121–5128.
15. Xu Y, Lu L, E LN, et al. Application of Radiomics in Predicting the Malignancy of Pulmonary Nodules in Different Sizes. AJR Am J Roentgenol 2019;213(6):1213–1220.
16. Cheng DT, Mitchell TN, Zehir A, et al. Memorial Sloan Kettering-Integrated Mutation Profiling of Actionable Cancer Targets (MSK-IMPACT): a hybridization capture-based next-generation sequencing clinical assay for solid tumor molecular oncology. J Mol Diagn 2015;17(3):251–264.
17. Martini N, Melamed MR. Multiple primary lung cancers. J Thorac Cardiovasc Surg 1975;70(4):606–612.
18. Amin MB, Greene FL, Edge SB, et al. The Eighth Edition AJCC Cancer Staging Manual: Continuing to build a bridge from a population-based to a more "personalized" approach to cancer staging. CA Cancer J Clin 2017;67(2):93–99.
19. von Elm E, Altman DG, Egger M, et al. The Strengthening the Reporting of Observational Studies in Epidemiology (STROBE) statement: guidelines for reporting observational studies. Ann Intern Med 2007;147(8):573–577.
20. Sanchez-Vega F, Mina M, Armenia J, et al. Oncogenic signaling pathways in the cancer genome atlas. Cell 2018;173(2):321–337.e10.
21. Rizvi H, Sanchez-Vega F, La K, et al. Molecular determinants of response to anti-programmed cell death (PD)-1 and anti-programmed death-ligand 1 (PD-L1) blockade in patients with non–small-cell lung cancer profiled with targeted next-generation sequencing. J Clin Oncol 2018;36(7):633–641.
22. Chakravarty D, Gao J, Phillips SM, et al. OncoKB: A Precision Oncology Knowledge Base. JCO Precis Oncol 2017;2017:PO.17.00011.
23. Suzuki K, Kusumoto M, Watanabe S, Tsuchiya R, Asamura H. Radiologic classification of small adenocarcinoma of the lung: radiologic-pathologic correlation and its prognostic impact. Ann Thorac Surg 2006;81(2):413–419.
24. Apte AP, Iyer A, Crispin-Ortuzar M, et al. Technical Note: Extension of CERR for computational radiomics: A comprehensive MATLAB platform for reproducible radiomics research. Med Phys 2018;45(8):3713–3720.
25. Zwanenburg A, Leger S, Vallières M, Löck S. Image biomarker standardisation initiative. ArXiv 1612.07003 [preprint] https://arxiv.org/abs/1612.07003. Posted December 21, 2016. Accessed June 14, 2021.
26. Isaka T, Yokose T, Ito H, et al. Correlations Between the EGFR Mutation Status and Clinicopathological Features of Clinical Stage I Lung Adenocarcinoma. Medicine (Baltimore) 2015;94(42):e1784.
27. Wu L, Gao C, Xiang P, Zheng S, Pang P, Xu M. CT-Imaging Based Analysis of Invasive Lung Adenocarcinoma Presenting as Ground Glass Nodules Using Peri- and Intra-nodular Radiomic Features. Front Oncol 2020;10:838.
28. Chen LW, Yang SM, Wang HJ, et al. Prediction of micropapillary and solid pattern in lung adenocarcinoma using radiomic values extracted from near-pure histopathological subtypes. Eur Radiol 2021;31(7):5127–5138.
29. Ji H, Ramsey MR, Hayes DN, et al. LKB1 modulates lung cancer differentiation and metastasis. Nature 2007;448(7155):807–810.
30. Facchinetti F, Bluthgen MV, Tergemina-Clain G, et al. LKB1/STK11 mutations in non–small cell lung cancer patients: Descriptive analysis and prognostic value. Lung Cancer 2017;112:62–68.
31. Skoulidis F, Goldberg ME, Greenawalt DM, et al. STK11/LKB1 mutations and PD-1 inhibitor resistance in KRAS-mutant lung adenocarcinoma. Cancer Discov 2018;8(7):822–835.
32. Scrima M, De Marco C, Fabiani F, et al. Signaling networks associated with AKT activation in non–small cell lung cancer (NSCLC): new insights on the role of phosphatydil-inositol-3 kinase. PLoS One 2012;7(2):e30427.
33. Hong DS, Fakih MG, Strickler JH, et al. KRASG12C inhibition with sotorasib in advanced solid tumors. N Engl J Med 2020;383(13):1207–1217.
34. Skoulidis F, Li BT, Dy GK, et al. Sotorasib for Lung Cancers with *KRAS* p.G12C Mutation. N Engl J Med 2021;384(25):2371–2381.
35. Kelsey I, Manning BD. mTORC1 status dictates tumor response to targeted therapeutics. Sci Signal 2013;6(294):pe31.
36. Misale S, Fatherree JP, Cortez E, et al. KRAS G12C NSCLC models are sensitive to direct targeting of KRAS in combination with PI3K inhibition. Clin Cancer Res 2019;25(2):796–807.